



ELSEVIER

Physica D 115 (1998) 29–48

PHYSICA D

The role of the spinodal region in one-dimensional martensitic phase transitions

A. Vainchtein^{a,*}, T. Healey^a, P. Rosakis^a, L. Truskinovsky^b

^a Department of Theoretical and Applied Mechanics, Cornell University, 212 Kimball Hall, Ithaca, NY 14853, USA

^b Department of Aerospace Engineering and Mechanics, University of Minnesota, Minneapolis, MN 55455, USA

Received 5 March 1997; received in revised form 12 August 1997; accepted 3 September 1997

Communicated by J.M. Ball

Abstract

A common approach in modeling martensitic phase transitions in the framework of continuum mechanics involves a nonconvex energy. This paper analyzes the influence of the *spinodal region*, or the region where the energy density is concave, on the resulting equilibria. We compare a one-dimensional model with a degenerate spinodal region to models with a finite spinodal region. In all models we consider an elastic bar with a nonconvex energy placed on a rigid elastic foundation, to mimic elastic interactions between different phases in higher dimensions. Interfacial energy is modeled by a strain-gradient term. We find that when the spinodal region is small, global minima are not affected, and the minimum energy as a function of the overall strain exhibits nonsmooth oscillations associated with sudden finite phase nucleation. However, a sufficiently wide spinodal region results in the partial smoothing of the global minimum energy and *infinitesimal phase nucleation in the interior* of the bar. This involves gradual growth of a *pretransitional* nucleus with strain in the spinodal region. We show a hysteresis path using an energetic strategy of switching between branches of local minima. Copyright © 1998 Elsevier Science B.V.

PACS: 64.70Kb; 64.80Gd; 81.30Kf; 83.10Ff

Keywords: Spinodal region; Phase nucleation; Pretransitional nucleus; Hysteresis

0. Introduction

Materials undergoing stress-induced martensitic phase transitions often form a variety of finely layered microstructures and exhibit hysteretic behavior [1,4,7,11,24,26].

In the last 20 years, a number of researchers have attempted to describe twinning, formation of microstructure and hysteresis in crystalline solids

within the framework of elasticity theory. A common approach involves minimization of a nonconvex elastic energy for the material. In his pioneering analysis of a one-dimensional elastic bar, Ericksen [9] has demonstrated the relevance of nonconvex energy in the modeling of crystalline solids exhibiting twin microstructures.

We consider a one-dimensional bar whose elastic energy density is a nonconvex two-well potential function of strain. The two wells represent two different material phases. The bar interacts with an elastic foundation. This interaction mimics the

* Corresponding author. Tel: (607) 255-9174; fax: (607) 255-2011; e-mail: vainchte@tam.cornell.edu.

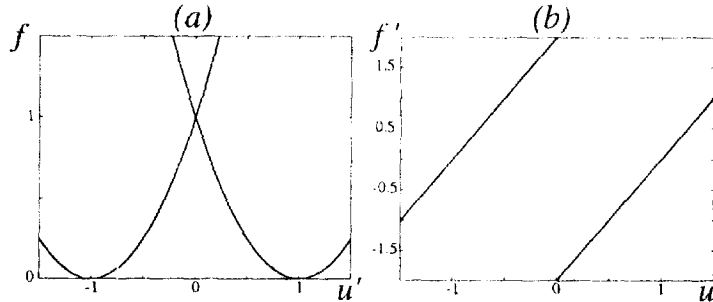


Fig. 1. Two-parabola model: (a) energy density; (b) stress.

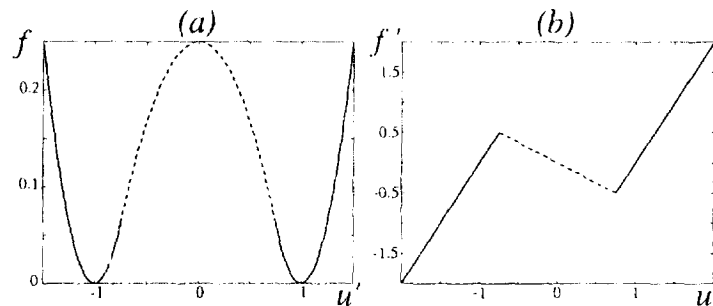


Fig. 2. Three-parabola model: (a) energy density; (b) stress.

three-dimensional boundary conditions constraining the surface displacements and induces microstructural refinement [3]. On the other hand, a strain-gradient term, intended to model interfacial energy, causes the system to minimize the number of interfaces [6]. The combined effect of these two terms in the total energy selects the number of interfaces in both local and global minimizers.

This approach has been considered by Müller [20,21] for a smooth two-well energy with zero displacement boundary conditions and by Truskinovsky and Zanzotto [29,30] for the case of multi-valued energy density represented by two convex (quadratic) functions (see Fig. 1) and general displacement boundary conditions.

For a smooth energy density $f(u')$, the *spinodal region* is the set of strains u' where f is locally concave, or $f'' < 0$. In the “two-parabola model” model by Truskinovsky and Zanzotto [29,30] the spinodal region reduces to a point separating two convex quadratic branches of f (the low- and high-strain phases).

This paper is concerned with the effect of the spinodal region on the structure of equilibria of the elastic bar. For analytical simplicity we adopt a “three-parabola model” with single-valued energy; f is piecewise quadratic with two intervals of convexity (low- and high-strain well) separated by a finite spinodal region (see Fig. 2). We compare the two- and three- parabola models and also consider a model with a smooth nonconvex f (Fig. 3).

As in [29,30], we are interested in local minimizers of the total energy functional. Although the usual approach involving absolute minimization of the total energy captures some basic features of the microstructures [13], it cannot account for hysteresis, which arises when the material gets locked in metastable states as suggested by calculations in [10,22]; see also [1,2,4,16,24].

Our approach relies on bifurcation analysis with respect to a loading parameter and enables us to study the evolution of branches of local minima. We find that the presence of the spinodal region yields a more

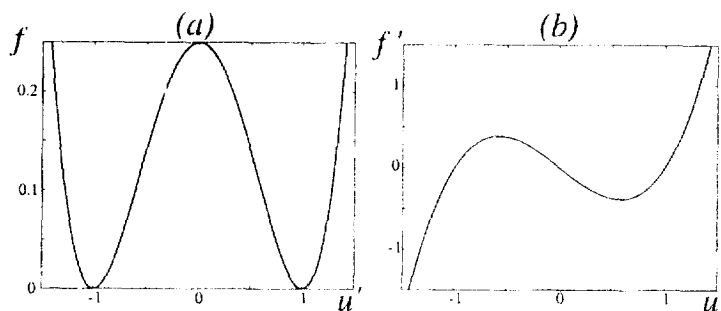


Fig. 3. Fully nonlinear model: (a) energy density; (b) stress.

complex bifurcation diagram. It is especially noteworthy that we find new types of nucleation patterns not observed in the two-parabola model. Our results show that global minima are not affected when the spinodal region is small. As in [30], the energy at the global minimum is not a smooth function of the prescribed average strain but exhibits corners. Each corner corresponds to a *finite nucleation event*. By that we mean the following: suppose that the bar is initially in the low-strain phase. At a critical value of average strain (corresponding to a corner in the lower energy envelope), an interval of *finite* length with strains in the high-strain phase suddenly appears in the interior of the bar. On the other hand, when the spinodal region is large enough, the lower energy envelope becomes partially smooth in the sense that some of the corners disappear. This gives rise to a different, *infinitesimal nucleation* process: as the load is increased, an initially infinitesimal interval with strains in the spinodal region appears in the bar interior and grows *gradually*. This *pretransitional* nucleus is stable although it involves strain in the spinodal region. Further load increase causes an initially infinitesimal high-strain interval to nucleate and grow within the pretransitional nucleus. An analogous type of infinitesimal nucleation can also occur at the ends of the bar.

We also find stable states with the entire bar in the spinodal region. The strains exhibit spatial oscillations approaching the high- and low-strain phases. This pattern is related to a pretransitional pattern known as *premartensite tweed*, which is experimentally observed; see [15] for a discussion. Further load increase results

in formation of a low- and high-strain mixture with pronounced phase boundaries.

These types of states involving strains in the spinodal region are a special feature of the present model. They are not possible in the two-parabola model or models without interfacial energy and elastic foundation effects.

We consider a strategy for switching between branches of local minima, that is energetically motivated and show that this procedure leads to hysteresis.

In Section 1 we motivate our choice of the energy functional by considering separately the effects of interfacial energy and elastic foundation terms. We formulate the relevant functional and necessary conditions for equilibria for the models in Section 2, and remark on the computation of the equilibria, while in Section 3 we discuss the issue of stability. Section 4 contains predictions based on bifurcation theory and perturbation analysis for small values of the foundation coefficient. In Section 5 we compare the calculated phase equilibria with a small number of interfaces for the three models and discuss the effects of the spinodal region. In Section 6 we consider a possible hysteresis scenario; Section 7 is devoted to conclusions.

1. Motivation

Consider a bar of unit undeformed length under prescribed end displacements (hard device). Let $x \in [0, 1]$ be the reference coordinate of a point in the

bar; $u(x)$ and $u'(x)$ are the displacement and strain at x , respectively. The total potential energy of the bar is given by [29,30]:

$$E = \int_0^1 [f(u') + \alpha(u'')^2 + \beta u^2] dx. \quad (1)$$

Here $\int_0^1 f(u') dx$ is the elastic energy stored in the bar, $\int_0^1 \alpha(u'')^2 dx$ models the interfacial energy and $\int_0^1 \beta u^2 dx$ is the energy of the elastic foundation. The significance of each of these terms is discussed below. We seek the local minimizers of the energy functional (1) subject to prescribed end displacements

$$u(0) = -d/2, \quad u(1) = d/2. \quad (2)$$

1.1. Ericksen's model

Ericksen [9] considered a problem of equilibrium for a nonlinearly elastic bar with nonconvex energy without strain-gradient or foundation terms ($\alpha = 0, \beta = 0$). The problem reduces to the minimization of the energy functional

$$E = \int_0^1 f(u') dx, \quad (3)$$

where $f(u')$ is a two-well elastic energy density. For example, we may consider

$$f(u') = \frac{1}{4}[(u')^2 - 1]^2 \quad (4)$$

shown in Fig. 3. The interval of strains $\{d: f''(d) \leq 0\}$, where f is locally concave, is called the *spinodal region*. In case of energy density given by (4), it is the interval $[-1/\sqrt{3}, 1/\sqrt{3}]$. By minimizing the functional (3) subject to the boundary conditions (2), Ericksen has shown that for d in $[-1, 1]$, apart from the homogeneous solution $u(x) = dx - \frac{1}{2}d$ which is unstable for d in $[-1/\sqrt{3}, 1/\sqrt{3}]$, there are infinitely many inhomogeneous solutions. These solutions are represented by a continuous displacement u describing a mixture of the two states $u' = \pm 1$ that minimize f (with the portion of the bar in each state prescribed

by d). All these solutions are global minimizers of the energy functional for d in the interval $[-1, 1]$.

1.2. Interfacial energy

One way to reduce this non-uniqueness of the equilibria is to introduce a strain-gradient term penalizing the formation of sharp interfaces:

$$E = \int_0^1 [f(u') + \alpha(u'')^2] dx, \quad (5)$$

where $\alpha > 0$ is a constant nonlocality coefficient. Solutions to the corresponding Euler–Lagrange equations are now smooth; all discontinuities in $u'(x)$ are replaced by smooth transition layers of thickness proportional to $\sqrt{\alpha}$. The idea of introducing this strain-gradient dependence has been widely used to analyze spinodal region decomposition, phase transitions and other phenomena (e.g. [6,19,28]).

In this case the Euler–Lagrange equation is given by

$$f''(u')u'' - 2\alpha u'''' = 0 \quad (6)$$

with the boundary conditions (2) and natural boundary conditions $u''(0) = u''(1) = 0$. This equation has the trivial solution (with constant strain $u' = d$):

$$u(x) = dx - \frac{1}{2}d. \quad (7)$$

A standard bifurcation analysis involving the linearization of (6) about (7) shows that branches of nontrivial solutions bifurcate from the trivial solution branch as d varies as a parameter. This occurs at the bifurcation points d_n that are solutions of

$$f''(d_n) = -2\alpha(\pi n)^2. \quad (8)$$

Along the n -branch (bifurcating from d_n), the solution is locally (near the bifurcation point)

$$u_n(x) = dx - \frac{1}{2}d + \varepsilon \sin(n\pi x) + o(\varepsilon) \quad (9)$$

as $\varepsilon \rightarrow 0$.

Assume that in the spinodal region $f''(d)$ monotonically decreases, reaches a negative minimum at some d_* ($d_* = 0$ for (4)) and then monotonically increases.

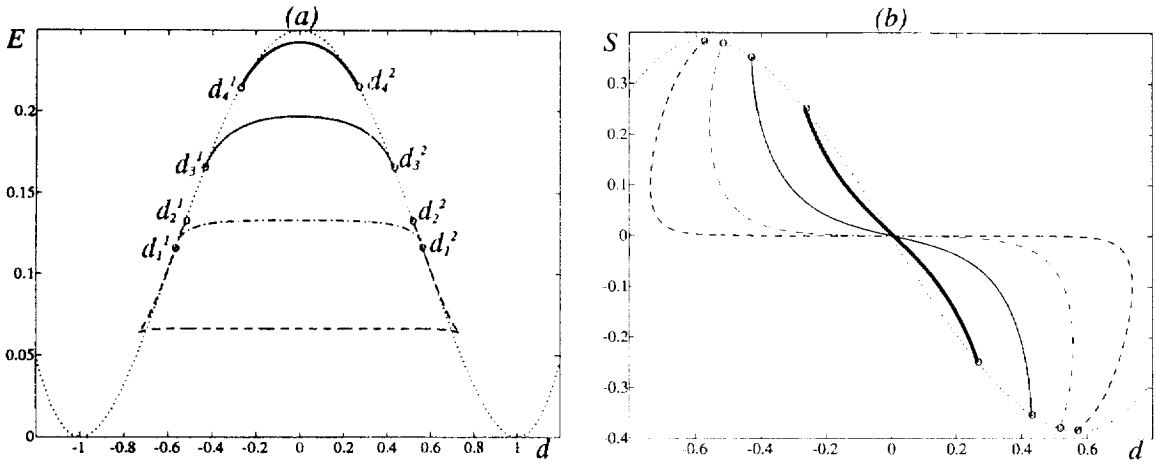


Fig. 4. (a) Energy and (b) stress diagrams ($S(d) = E'(d)$) for Ericksen’s problem with interfacial energy added: $\alpha = 0.0025$; dotted line: $n = 0$, dashed line: $n = 1$, dash-dotted line: $n = 2$, solid line: $n = 3$, thick solid line: $n = 4$.

This will cause the bifurcation points d_n to come in pairs, $d_n^1 < d_*$ and $d_n^2 > d_*$ such that $d_n^{1,2}$ both satisfy (8) for the same n . One shows that d_n^1 and d_n^2 correspond to the same branch. Moreover, the bifurcation points are ordered: $d_n^1 < d_m^1, d_n^2 > d_m^2, m < n$. The number of bifurcation points is then

$$n_{\max} = \left\lfloor \frac{1}{\pi} \sqrt{\frac{|f''(d_*)|}{2\alpha}} \right\rfloor, \tag{10}$$

where $\lfloor a \rfloor$ denotes the largest integer less than a . Hence n_{\max} increases as one increases $|f''(d_*)|$ (thus sharpening the spinodal region peak) or decreases α . For any smooth two-well potential $f(u')$, n_{\max} is finite as long as $\alpha \neq 0$.

As interesting consequence of (10) is that it implies $n_{\max} = \infty$ when the $f(u')$ is given by two parabolae – the case studied in [30]. Indeed, consider a sequence of C^2 functions $f_i(u')$ converging as $i \rightarrow \infty$ to the piecewise smooth function $f(u')$ whose graph consists of two parabolae meeting at $u' = d_*$. For each of the functions f_i in the sequence (10) gives some $n_{\max,i}$ that increases with $f_i''(d_*)$, hence tends to infinity as $i \rightarrow \infty$. Also, one can see from (8) that as i grows, the bifurcation points d_n tend to cluster near d_* and in the limit (i.e. in the two-parabola model) they all coincide at $d_n = d_*$. This explains why in [30] $d = d_*$ is a singular point from which all the branches bifurcate.

Eq. 6 can be integrated in quadratures and so the nontrivial solutions can be found analytically [23,28].

The resulting energy-versus-end displacement diagram (for f as in (4)) is shown in Fig. 4(a). The energy density is symmetric, so $d_n^2 = -d_n^1$ and $d_* = 0$. The number of bifurcating branches in this particular case is $n_{\max} = 4$.

We remark on the meaning of the number n . Along the n -branches of solutions depicted in Fig. 4, at sufficiently small d , the strains $u'_n(x)$ have n zeroes. As the nonlocality coefficient α tends to 0, these solutions approach solutions of Ericksen’s problem with $\alpha = 0$ [9]. In these limiting solutions the strain $u'_n(x)$ alternates between the values 1 and -1 , with n jumps. Therefore, one can view n as the number of phase boundaries. Note also that by (10), n_{\max} tends to ∞ as α tends to 0; we know from [9] that if $\alpha = 0$ there is no upper limit on the number of phase boundaries.

Fig. 4 shows that the smaller the n is, the lower is the energy of the corresponding solution branch. In fact, the solution with one interface is the global minimum, while others are not even local minimizers [6]. However, experimental results [7] show that solutions with multiple interfaces are often preferred.

1.3. Elastic foundation

Another approach is based on the observation that multiple interface microstructures arise in higher

dimensional settings, where the displacement is much more severely constrained by the boundary conditions than in one dimension. In order to model “the surrounding medium” the bar is placed on an elastic foundation (a continuous system of noninteracting, linearly elastic springs). Consider minimizing

$$E = \int_0^1 [f(u') + \beta u^2] dx \quad (11)$$

subject to the boundary conditions (2). Here the constant $\beta > 0$ is the stiffness of the foundation. For the case $d = 0$ it is well known that the infimum of E in $W_0^{1,4}(0, 1)$ is zero [3,31]. Here $W_0^{1,4}(0, 1)$ is the space of functions that are in $L^4(0, 1)$ together with their first weak derivatives and vanish at the ends. One can construct piecewise linear (sawtooth) minimizing sequences $u_k(x)$ with $u'_k(x) = \pm 1$ almost everywhere, with u_k tending to 0 uniformly, but the minimum is not attained, since the conflicting requirements $u' = \pm 1$ and $u = 0$ cannot be met simultaneously.

Equilibria for (11) can be found analytically (this was done in [3] for the special case of $d = 0$). As in Ericksen’s problem, one looks for solutions with continuous displacement but strains that are discontinuous at finite isolated points $c_i, i = 1, n$. We require that the strains alternate between the “+” and “−” phases (the intervals $(-\infty, -1/\sqrt{3})$ and $(1/\sqrt{3}, \infty)$ where $f(u')$ is convex), so that

$$f''(u') > 0 \quad (12)$$

holds in each $[c_i, c_{i+1}]$ interval. Any solution with strain in the spinodal region is unstable by Legendre’s necessary condition. In the intervals $[c_i, c_{i+1}]$ the Euler–Lagrange equation

$$f''(u')u'' - 2\beta u = 0 \quad (13)$$

should hold with the constraint (12). At the corner points c_i , Weierstrass–Erdman corner conditions are

$$[[f'(u')]]_{c_i} = 0, \quad (14a)$$

$$[[f(u') - f'(u')u']]_{c_i} = 0. \quad (14b)$$

Conditions (14b) stem from variations in c_i , while (13) and (14a) is obtained by varying u with positions of c_i fixed. In addition, boundary conditions and the continuity of displacement at the corners must be satisfied by equilibria.

Note that (14) means that at each corner the strain jumps from one Maxwell strain to another. These are the two values of strain e_1 and e_2 at which a straight line is tangent to both convex branches of the $f(u')$ graph; here, $e_1 = e_2 = 1$. The Euler–Lagrange equation (13) has the first integral

$$f(u') - f'(u')u' + \beta u^2 = \text{const.}$$

and can be integrated in quadratures since the function $g(u') = f(u') - f'(u')u'$ is invertible when (12) holds.

Fig. 5 shows the calculated equilibria. All branches shown are weak local minima of the energy functional (i.e. stable under smooth perturbations). However, they are unstable with respect to nucleation (perturbations with new interfaces close to each other) and so they are not strong local minima. The energy diagram illustrates the fact that the functional (11) possesses no global minimum: the energy decreases with n , approaching the infimum but an infinite number of interfaces (jumps) is needed to reach the limit.

2. Conditions for equilibrium

The goal of this work is to study the effects of the spinodal region in the elastic energy density f in the combined model (1). The latter involves both oscillation-inducing terms (elastic foundation) and oscillation-inhibiting (strain-gradient) terms; it is the interplay of these two terms that selects a finite number of interfaces in global or local minimizers.

We compare three models of the stored energy density f in (1).

2.1. Two-parabola model (bilinear material) [30]

The energy density is double-valued:

$$f(u') = \begin{cases} f_+(u'), \\ f_-(u'). \end{cases} \quad (15)$$

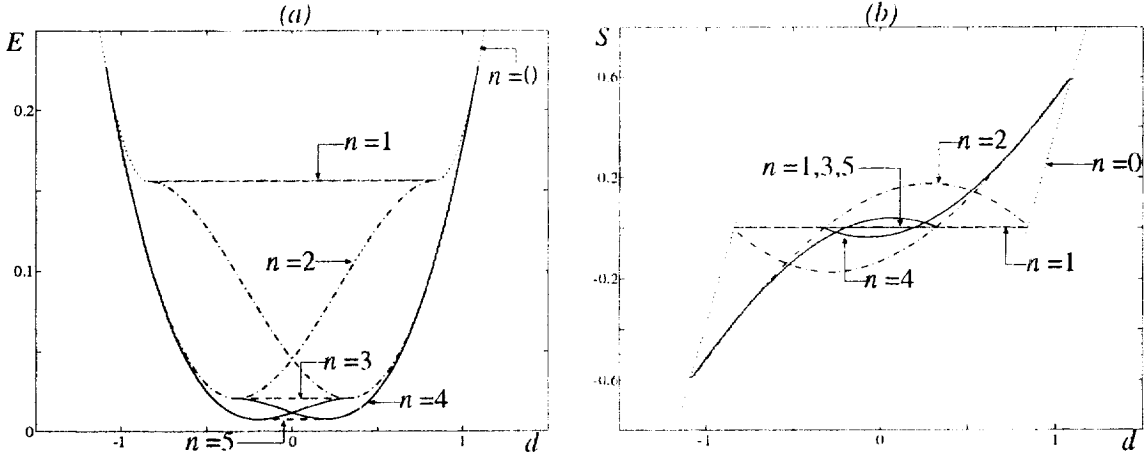


Fig. 5. (a) Energy $E(d)$ and (b) effective stress $S(d) = E'(d)$ diagrams for Ericksen's bar on elastic foundation of stiffness $\beta = 2.3$, without interfacial energy.

At each point it can be on either of two convex branches f_- and f_+ associated with two phases of the material labeled “+” and “-”. These are chosen to be

$$f_{\pm}(u') = (u' \pm 1)^2. \tag{16}$$

Plots of these functions and the corresponding stress-strain relations given by $\sigma_{\pm}(u') = f'_{\pm}(u')$ are shown in Fig. 1. Each portion of the bar is assumed to be occupied by either “+” or “-” phases but not both. It is shown in [30] that the associated equilibria are the same as with the single-valued energy density $f(u') = \min[f_+(u'), f_-(u')]$ which is a two-parabola approximation of a smooth two-well energy density. However, we remark that major differences arise between the three-dimensional analogs of the single-valued (see [18,25] and double-valued versions (15) (see [14]). Note that the spinodal region degenerates here to the point where the two parabolae intersect.

We assume that each phase occupies a *finite* union of intervals. This means that there is a finite number n of *transition points* $c_i, c_i < c_{i+1}$, in $(0, 1)$ where switching between phases occurs. Each c_i marks a location of a *phase boundary*.

Note that the double-valuedness of (15) allows extra degrees of freedom: in addition to smooth variations in u , one can also vary the positions of the phase boundaries c_i .

In order to test $[u, c_i]$ under the boundary conditions (2), fix n and consider the one-parameter family of competitors $X(x, \varepsilon) = x + \varepsilon\delta x(x)$ and $U(X, \varepsilon) = u(x + \varepsilon\delta x) + \varepsilon\delta u(x)$, with $\delta x(0) = \delta x(1) = \delta u(0) = \delta u(1) = 0$. Variation $\delta x(x)$ displaces the transition points c_i to the new positions $C_i = c_i + \varepsilon\delta x(c_i)$. By requiring $\delta u(x)$ to be C^1 , piecewise C^2 and $\delta x(x)$ to be C^2 , one can obtain the following necessary conditions for the equilibria [30]. The displacement $u(x)$ must be in $C^1[0, 1]$, C^4 in the intervals $[c_i, c_{i+1}]$, $i = 0, \dots, n$. In each interval the Euler–Lagrange equation

$$2\alpha u'''' - f''(u')u'' + 2\beta u = 0 \tag{17}$$

must be satisfied. Here $f = f_+$ or f_- depending on what phase occupies the given interval. In addition we have natural boundary conditions

$$u''(0) = u''(1) = 0, \tag{18}$$

stress continuity conditions

$$[[f'_{\pm}(u') - 2\alpha u''']]_{c_i} = 0, \tag{19}$$

(note that the stress includes the derivative of the *couple stress* $2\alpha u''$), couple stress continuity

$$[[u''']]_{c_i} = 0, \tag{20}$$

and the corner condition

$$[[f_{\pm}(u')]]_{c_i} = 0. \quad (21)$$

Here (17)–(20) come from variations of the elastic field, while (21) is due to variations of the transition points. It means that the strain $u'(c_i)$ at a transition point must equal the strain at which f_+ and f_- intersect. In addition, the smoothness conditions

$$[[u']]_{c_i} = [[u]]_{c_i} = 0 \quad (22)$$

and the boundary conditions (2) must be satisfied.

2.2. Three-parabola model (trilinear material)

In this model f is single-valued and given by

$$f(u') = \begin{cases} f_+(u') = (u' + 1)^2 & \text{for } u' \leq -t, \\ f_0(u') = \gamma(u')^2 + \eta & \text{for } -t < u' < t, \\ f_-(u') = (u' - 1)^2 & \text{for } u' \geq t, \end{cases} \quad (23)$$

where

$$\gamma = 1 - 1/t < 0 \quad \eta = 1 - t$$

and $t, -t$ are the points of contact of the three parabolas. This function, as well as the corresponding stress-strain curve, is shown in Fig. 2. The parameters γ and η are chosen so that f is C^1 . This results in an approximation of a fully nonlinear two-well energy density.

As in the two-parabola model, we assume that there is a finite number n of isolated transition points c_i . The strain-gradient term $\alpha u''^2$ enforces continuity of the strain $u'(x)$. The continuity of u' and the single-valuedness of f restrict the location of transition point c_i by the condition

$$u'(c_i) = \pm t, \quad (24)$$

where the sign depends on whether c_i separates “–” and “0” regions or “+” and “0” regions.

We require the admissible variations in $u(x)$ to be in $H^2(0, 1)$ and satisfy the zero boundary conditions. Hence variations are $C^1[0, 1]$ and their second distributional derivatives are square integrable in $[0, 1]$. We then obtain the following necessary conditions for equilibria. The equilibrium displacement $u(x)$ must be a $C^3[0, 1]$, piecewise C^4 function, with the Euler–Lagrange equation (17) satisfied in each interval

$[c_i, c_{i+1}]$. Here f has subscript +, 0 or – depending on which phase occupies $[c_i, c_{i+1}]$. Observe that intervals in the “+” and “–” phases must be separated by an interval in the “0” phase (spinodal region). In addition, equilibria must satisfy the boundary conditions (2), the natural boundary conditions (18), the smoothness conditions (22), couple stress continuity (20) and stress continuity (19). Since f and u are C^1 , stress continuity (19) reduces to

$$[[u''']]_{c_i} = 0. \quad (25)$$

When the specific forms of (15) and (23) are used, the jump conditions (19), (20) and (22) for the two-parabola model reduce to

$$\begin{aligned} [[u]]_{c_i} = 0, \quad [[u']]_{c_i} = 0, \quad [[u'']]_{c_i} = 0, \\ [[\alpha u'' + \text{sgn}(u')]]_{c_i} = 0, \end{aligned} \quad (26)$$

while the corner condition (21) reduces to

$$u'(c_i) = 0. \quad (27)$$

In the three-parabola case, (26) is replaced by

$$\begin{aligned} [[u]]_{c_i} = 0, \quad [[u']]_{c_i} = 0, \\ [[u'']]_{c_i} = 0, \quad [[\alpha u''']]_{c_i} = 0 \end{aligned} \quad (28)$$

and location of c_i is restricted by (24).

The Euler–Lagrange equation (17) in the \pm phase intervals (both models) and in 0 intervals (spinodal region; three-parabola) reduce to linear ordinary differential equations with constant coefficients in view of (15) and (23): in + and – intervals,

$$\alpha u'''' - u'' + \beta u = 0, \quad (29)$$

while in 0 intervals,

$$\alpha u'''' - \gamma u'' + \beta u = 0. \quad (30)$$

The displacement in the i th interval $[c_i, c_{i+1}]$ is a linear combination of four functions with hitherto undetermined constants $a_{k,i}$, $k = 1, \dots, 4$. The specific form depends on the sign of $1 - 4\alpha\beta$ for \pm intervals and the sign of $\gamma^2 - 4\alpha\beta$ for 0 intervals. It involves polynomial, exponential, trigonometric functions and combinations thereof in each case.

The coefficients $a_{k,i}$ are then found by matching the solutions in the intervals by means of jump conditions

(given by (26) for two parabolae and by (28) for three parabolae) and using the boundary conditions (2) and (18). This yields a linear system of equations for $a_{k,i}$.

To find the extremals of the energy functional at fixed n , one has to find c_i from (27) and (24) for the two- and three-parabola cases, respectively. This results in a nonlinear algebraic system.

We first solve the linear system for $a_{k,i}(c_i, d, \alpha, \beta, \gamma)$ and then substitute the result into the nonlinear system to solve for c_i as nonlinear functions of d, α, β and γ . The solutions are not unique so that the functions $c_i(d, \alpha, \beta, \gamma)$ are multi-valued. Typically there is more than one equilibrium for a given end displacement d and the number of interfaces n .

2.3. Fully nonlinear model

Here f is a smooth function with two wells and a spinodal region (see Fig. 3):

$$f(u') = \frac{1}{4}(u'^2 - 1)^2. \quad (31)$$

Equilibria $u(x)$ must satisfy the Euler–Lagrange equation (17) with boundary conditions (2) and (18). Here we assume the competitors to be in $H^2(0, 1)$. A standard argument shows that the equilibria belong to $C^4[0, 1]$.

Eq. (17) is now a nonlinear fourth-order ordinary differential equation with α, β and d as parameters. It is solved numerically using the pseudo-arclength continuation technique implemented in the software package AUTO [8] with the displacement d treated as the continuation parameter. The program follows the main branch of solutions determining the bifurcation points (where other branches emerge) and then calculates the bifurcating branches.

3. Stability

For the two-parabola model, the problem of stability is essentially finite-dimensional [30]. One first minimizes the total energy for fixed number n and locations c_i of interfaces. This is facilitated by the double-valued special form of f . The resulting expression of the energy for fixed n depends on the variables c_i . Min-

imization with respect to c_i yields different branches of local minima for given d . The energies for different n can then be compared directly to examine global minima. See [30] for details.

In the three-parabola model the study of stability does not reduce to a finite-dimensional problem. The transition points c_i are no longer independent variables since the strain is continuous across them and $u'(c_i) = \pm t$.

Therefore, we consider the second variation of the energy functional directly

$$\delta^2 E(u_0; \eta) = \int_0^1 [f''(u'_0)(\eta')^2 + 2\alpha(\eta'')^2 + 2\beta\eta^2] dx, \quad (32)$$

where $\eta(x) \in H_0^2(0, 1) = \{h(x) \in H^2(0, 1): h(0) = h(1) = 0\}$ is a variation and $u_0(x)$ is an extremal, i.e. $\delta E(u_0, \eta) = 0$ for any η in $H_0^2(0, 1)$. For $f(u')$ given by (23), $f''(u')$ in (32) is piecewise constant with jumps at $u' = \pm t$. Using the assumption that $u'_0(x)$ has a finite number of isolated points c_i where $u'_0(c_i) = \pm t$ (so that it is strictly monotone in some neighborhoods of c_i) and taking into account the continuity of $u'_0(x)$, one can show that the second variation is continuous at u_0 uniformly with respect to η in $H_0^2(0, 1)$. In view of this, the strict positive definiteness of the second variation, that is, existence of constant $k > 0$ such that

$$\delta^2 E(u_0; \eta) \geq k \|\eta\|_{H^2(0,1)}^2,$$

is sufficient for $u_0(x)$ to be a local minimum with respect to our admissible variations (see [32, Theorem 40A]). For the simple cases with no phase boundaries the stability analysis can be done analytically. When phase boundaries are present and α and β satisfy $4\alpha\beta \leq \gamma^2$ we approximate the variation $\eta(x)$ by cubic Hermite polynomials, so that the second variation (32) is approximated by a finite sum, and investigate the sign of the minimal eigenvalue of the resulting quadratic form. In case $\gamma^2 - 4\alpha\beta < 0$ it can be shown [17] that the energy functional is convex and at each value of d there exists a unique equilibrium global minimizer.

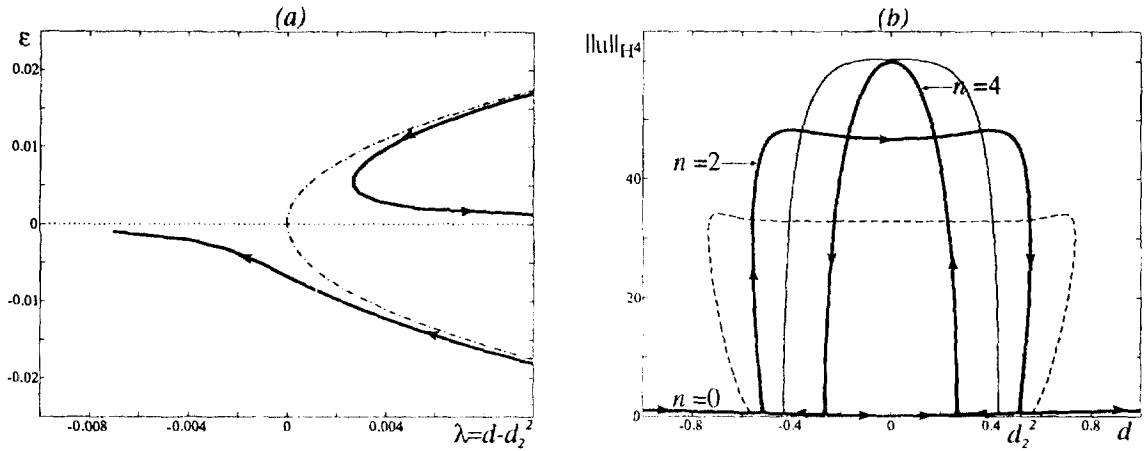


Fig. 6. (a) Local bifurcation diagram from imperfection analysis: $\alpha = 0.0025$. Dotted line: $n = 0$ at $\beta = 0$, dash-dotted line: $n = 2$ at $\beta = 0$, thick solid line: $n = 0, 2$ at $\beta = 0.005$. (b) Global bifurcation diagram obtained numerically: $\alpha = 0.0025, \beta = 0.005$. Thick solid line: $n = 0, 2, 4$ (the main branch), dashed line: $n = 1$, solid line: $n = 3$.

Stability for the fully nonlinear model was studied numerically by the same method.

The results are shown in Section 5.

4. Symmetry and local perturbation results

As was pointed out in [30], we have two types of symmetry: (i) Geometric symmetry (“G-symmetry”): if $u_d(x)$ is an equilibrium solution satisfying (17), (2) and (18) then so is $v_d(x) = -u_d(1-x)$, with the same total energy. We refer to solutions satisfying

$$u(x) = -u(1-x) \tag{33}$$

as *G-symmetric*. Solutions for which (33) does not hold are called *non-G-symmetric* and come in pairs. (ii) Physical symmetry: if $u_d(x)$ is an equilibrium for given d and the energy density satisfies $f(-u') = f(u')$, then so is $v_{-d}(x) = -u_d(x)$, with the same energy. The total energy is thus an even function of d : $E(d) = E(-d)$.

In Section 1 we considered the special case $\beta = 0$ ($\alpha \neq 0$) and have shown the energy and stress diagrams in Fig. 4. For $\beta > 0$ and $d \neq 0$ the trivial solution (7) of problem (6) ($\beta = 0$) no longer satisfies the Euler–Lagrange equation (17) with nonzero β . However, a local perturbation analysis with β as the

perturbation parameter shows that the main branch solutions of the perturbed problem will follow the branches with *even* n of the unperturbed ($\beta = 0$) problem near the points where these branches bifurcate. Consider bifurcation point d_2^2 in the energy diagram shown in Fig. 4(a). When $\beta = 0$, one can show that near this point

$$d = d_2^2 + B\varepsilon^2 + o(\varepsilon^2),$$

$$\varepsilon = \int_0^1 \sqrt{2} \sin(2\pi x) (u - dx + \frac{1}{2}d) dx,$$

where B is a constant. The corresponding local ε – d bifurcation diagram for $n = 2$ (dash-dotted line in Fig. 6(a)) is a pitchfork bifurcation. As we introduce a small perturbation $\beta > 0$, we obtain instead,

$$d = d_2^2 + A \frac{\beta}{\varepsilon} + B\varepsilon^2 + C\beta$$

$$+ D \frac{\beta^2}{\varepsilon^2} + o(\varepsilon^2) + o\left(\frac{\beta^2}{\varepsilon^2}\right),$$

where A, B, C, D are constants for which analytical expressions are available. The corresponding diagram is shown by a thick solid line in Fig. 6(a). A similar diagram can be obtained for $n = 4$.

The global bifurcation diagram obtained numerically is shown in Fig. 6(b). Locally it agrees with the analytical results. Thus, the bifurcation points of even n branches in the unperturbed problem get replaced by turning points in the perturbed one while bifurcation points of the odd branches do not. Using arguments from [12] one can easily show that there is a G-symmetric solution branch connected to the solution $u = 0, d = 0$. Hence the main branch consists of G-symmetric solutions, and non-G-symmetric solutions form the bifurcating branches. Solutions along bifurcating branches with even- n in the unperturbed problem possess G-symmetry while solutions with odd- n do not. Thus, in our example with $n_{\max} = 4$ when $\beta = 0$, the main branch in the perturbed problem follows the trivial solution $n = 0$ (coming from the negative d direction), then makes a turn and goes close to the $n = 2$ branch of the unperturbed problem, again follows $n = 0$, makes another turn to follow $n = 4$, goes close to $n = 0$ again, follows $n = 4$, then $n = 0$, goes close to $n = 2$ and then turns to $n = 0$ in the positive d direction. From this main branch other branches of solutions with less symmetry bifurcate ($n = 1, 3$ in this example). See Fig. 6(b). The sketch of the energy diagram is given in Fig. 7 (compare to Fig. 4).

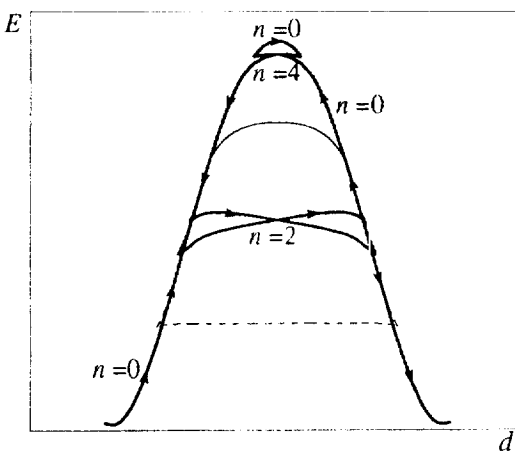


Fig. 7. Sketch of the energy diagram with small elastic foundation coefficient: dashed: $n = 1$, solid: $n = 3$, thick solid: $n = 0, 2, 4$.

5. Comparison of the three models

We compare phase equilibria with a low number of interfaces in all three models.

Following [30], we choose α, β and t that satisfy both $\gamma^2 - 4\alpha\beta > 0$ and $1 - 4\alpha\beta > 0$ (recall that $2t$ is the width of the spinodal region and $\gamma = 1 - 1/t$). Recall that in the case $\gamma^2 - 4\alpha\beta < 0$ the energy functional is convex [17]. Thus at each d there is a unique equilibrium which is also the global minimizer. Hence hysteresis cannot take place. This was also observed in numerical calculations. The energy functional in the two-parabola model is never convex because $\gamma = -\infty$, and so $4\alpha\beta < \gamma^2$. Finally, when $\alpha\beta \gg 1$ no microstructures are observed.

Formula (10) shows that in the case $\beta = 0$ the maximum number n_{\max} of zeroes of strain in bifurcating branches is determined by the nonlocality coefficient α and by the curvature of the spinodal region near its peak $f''(0) = 2\gamma$. The results of our computations suggest that the elastic foundation does not change n_{\max} and formula (10) apparently holds for nonzero β as well. Notice that by (10) n_{\max} tends to ∞ as α tends to 0, and we have seen in Section 1 that $n_{\max} = \infty$ when $\alpha = 0$ but $\beta \neq 0$.

On the other hand, the stability and shape of branches depends on all of α, β and t .

The results of calculations are presented in two kinds of diagrams: total energy $E(d)$ and effective stress $S(d) = E'(d)$. One can show that $S(d)$ equals the end stress (at $x = 0, 1$). The stability of the computed solutions is indicated in figure captions.

5.1. The interfaces

The notions of a phase boundary in the models with spinodal region and in the two-parabola model are different. In the two-parabola model [30] + and - intervals are consecutive. However, in models with spinodal region there is a “thick interface” between the phase: the + and - intervals are always separated by a 0 (spinodal region) interval, e.g. (+, 0, -) as opposed to (+, -). The notation (+, 0, -) means that the three intervals $[0, c_1], [c_1, c_2]$ and $[c_2, 1]$ are occupied by the +, 0 and - phase, respectively. Thus in place of

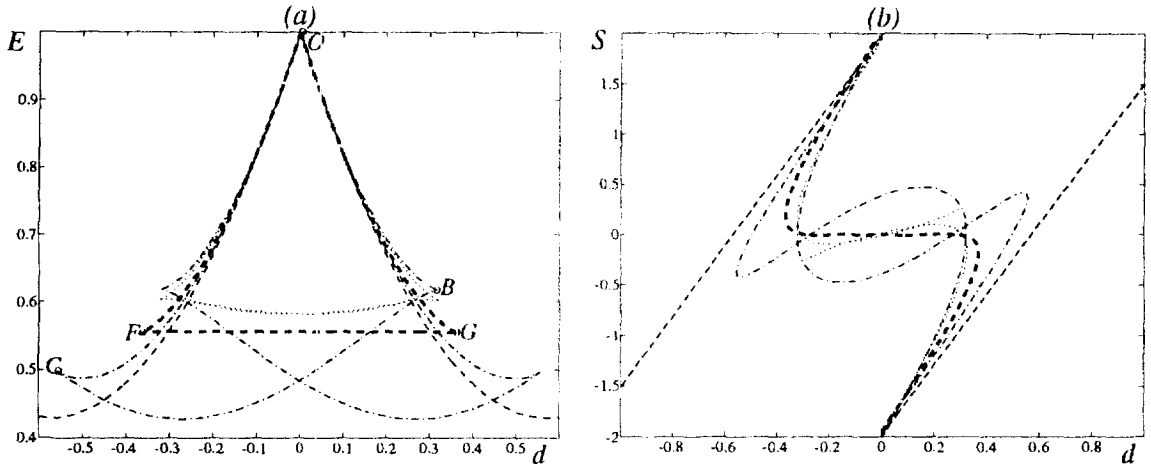


Fig. 8. (a) Energy $E(d)$ and (b) effective stress $S(d)$ diagrams for the two-parabola model (from [30]): $\alpha = 0.01$, $\beta = 10$; dashed: $n = 0$ (stable), boldly dashed: $n = 1$ (FG is stable, OG and OF are unstable), dash-dotted: $n = 2$, G-symmetric (BC is stable, OB and OC unstable), dotted: $n = 2$, non-G-symmetric (unstable).

one phase boundary in two-parabola case there are two transition points or one “thick” boundary for models with the spinodal region.

Moreover, with the spinodal region now present, new combinations of phases arise, e.g. $(0, -, 0)$, $(+, 0, +)$ and $(+, 0)$. As we shall see, these solutions form “transitional” branches connecting the 0-branches (without phase boundaries) with branches having “true” interfaces where the spinodal region separates two different phases.

5.2. The 0-branch of phase equilibria

In the two-parabola model, solutions with no transition points ($(+)$ or $(-)$) are solutions of (29) subject to (2) and (18). The resulting branches are represented by a dashed curve in Fig. 8. When the spinodal region is present, the 0-branch is *not defined for all* d but consists of three separate parts (see Fig. 12 and Figs. 9–11). The left and right parts are branches of solutions of (29) with strain $u' < -t$ and $u' > t$ ($(+)$ and $(-)$, respectively). The middle part is the branch of solutions of (30) with $-t \leq u' \leq t$ (spinodal region). These parts get closer to each other as we decrease β . Physically the separation of these 0-branches means that only if one pulls far enough one gets a pure \pm

phase solution. This is due to the elastic foundation. However, in the absence of a spinodal region pure phase solutions exist and are stable for all d (although not absolute energy minima for small d). In all models 0-branches have relatively high energy because of the elastic foundation.

5.3. The 2-branches of phase equilibria

5.3.1. G-symmetric branches

Dash-dotted curved triangles in Fig. 8 are G-symmetric $n = 2$ branches $((-, +, -)$ and $(+, -, +)$) calculated for the two-parabola model.

Corresponding branches in the models with spinodal region are all G-symmetric of type $(+, 0, -, 0, +)$, $(0, -, 0)$ and $(+, 0, +)$ (and corresponding types with $-$ and $+$ interchanged). The first type gives branches with two “true” (thick) interfaces (we call them “ $n = 2$ ” although there are four transition points). They are connected to the 0-branches and other branches with even n via the other two “transitional” branches of type $(0, -, 0)$ and $(+, 0, +)$.

To see how the spinodal region affects the $n = 2$ branches, we start with a two-parabola model ($t = 0$) and gradually insert a wider and wider spinodal region by increasing t , the maximum value of the energy E

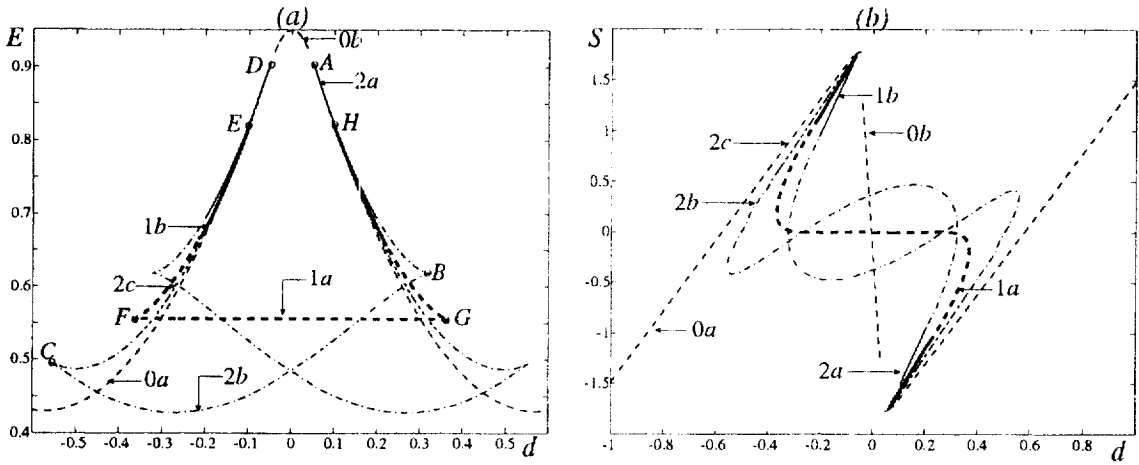


Fig. 9. (a) Energy $E(d)$ and (b) effective stress $S(d)$ diagrams for the three-parabola model: $\alpha = 0.01$, $\beta = 10$, $t = 0.05$; 0a: (+) (stable), 0b: (0) (unstable), 1a: $(-, 0, +)$ (FG is stable, the rest is unstable), 1b: $(0, +)$ (unstable), 2a: $(0, -, 0)$, G-symmetric (unstable), 2b: $(+, 0, -, 0, +)$, G-symmetric (BC is stable, the rest is unstable), 2c: $(+, 0, +)$, G-symmetric (unstable). Not all branches are shown.

becoming smaller (see Figs. 8–11). At $t = 0$ the $n = 2$ G-symmetric branch $((+, -, +)$, for example) has the form of a curved triangle (dash-dotted curve in Fig. 8). It is represented by OBC in Fig. 15. As we increase t (spinodal region width), the triangle opens up so that sides AB and CD emerge from two different points (A and D in Fig. 15) rather than a single point O . Also, the ends of the sides AB and CD are now occupied by $(0, -, 0)$ and $(+, 0, +)$ while the rest of the curve is $(+, 0, -, 0, +)$. Notice that while the point C is a turning point in Figs. 8–10, it is not as we increase t to 0.4 (see Fig. 11). Neither B nor C are turning points for $t = 0.75$ (Figs. 13 and 14). For large t the order of C and D is reversed, so that the 2-branch does not coexist with, but rather follows the 0-branch as d increases. This unfolding for large t is shown in Fig. 15. Along the $n = 2$ branch the following sequence is observed:

$$\begin{aligned}
 (+) &\longrightarrow (+, 0, +) \longrightarrow (+, 0, -, 0, +) \\
 &\longrightarrow (0, -, 0).
 \end{aligned}$$

This means that if we start increasing d from a negative value with only the + phase present, we observe first a 0 interval and then the - phase growing in the middle. The transition points move outward and the

+ phase disappears from the ends. If $f''(0)/(2\alpha) = (1 - 1/t)/\alpha$ is such that $2 \leq n_{\max} < 4$ in (10), this sequence of transitions can be continued as

$$(0, -, 0) \longrightarrow (0),$$

and the 2-branch connects to the spinodal region part of the 0-branch. See Figs. 11, 13 and 14. However, if branches with higher even n are present, which is the case in Figs. 9 and 10, the 2-branch connects to the spinodal region 0-branch via these branches with higher n . These branches were not calculated for the cases $t = 0.05$ and $t = 0.25$ but an example of such a connection can be seen in Figs. 6(b) and 17.

In fact, our calculations for the fully nonlinear model have shown that the 0-branch and all G-symmetric branches form the *main branch* of solutions. That is, the G-symmetric 2-branch does not bifurcate from the 0-branch but is in fact part of the main branch of solutions from which the branches with less symmetry bifurcate. This result is not seen in the two-parabola model because there all branches emerge from $d = 0$. In general, the main branch contains all G-symmetric solutions with even n . For example, in Fig. 17 it consists of G-symmetric solutions with $n = 0, 2, 4$.

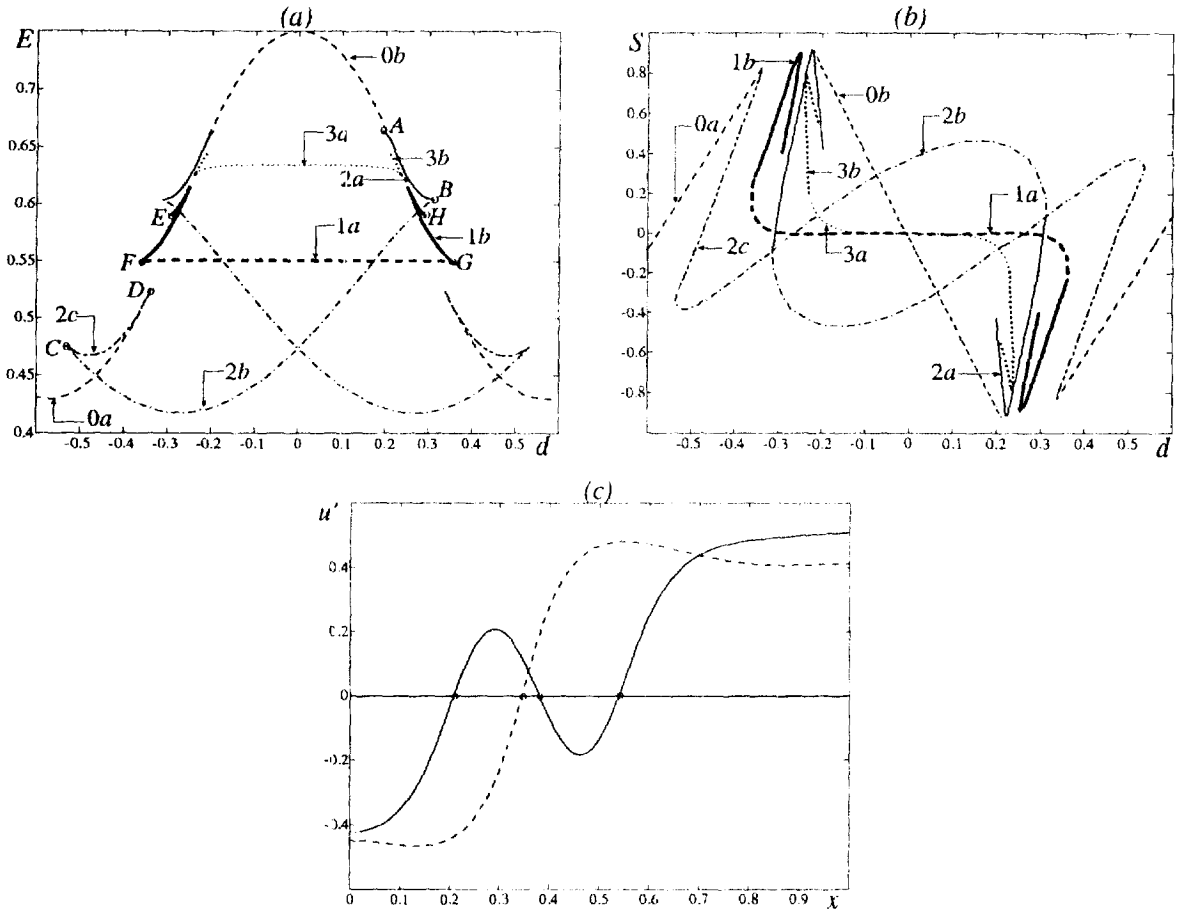


Fig. 10. (a) Energy $E(d)$ and (b) effective stress $S(d)$ diagrams for the three-parabola model: $\alpha = 0.01$, $\beta = 10$, $t = 0.25$; $0a$: (+) (stable), $0b$: (0) (unstable), $1a$: $(-, 0, +)$ (FG is stable, the rest is unstable), $1b$: $(0, +)$ (unstable), $2a$: $(0, -, 0)$, G-symmetric (unstable), $2b$: $(+, 0, -, 0, +)$, G-symmetric (stable), $2c$: $(+, 0, +)$, G-symmetric (unstable), $3a$: $(-, 0, +)$, $n = 3$ (unstable), $3b$: $(0, +)$, $n = 3$ (unstable); (c) solutions at the same value of d belonging to different $(-, 0, +)$ -branches. The solid ($n = 3$) and dashed ($n = 1$) curves represent the strains on the branches $3a$ and $1a$ correspondingly.

One can observe how the unfolding of the symmetric $n = 2$ branch with increasing t leads to *smoothing* of the lower envelope of the $n = 0$ and $n = 2$ branches. Indeed, at $t = 0$, $t = 0.05$ and $t = 0.25$ (Figs. 8–10) this envelope is *ncnsmooth*: the branches $n = 0$ and $n = 2$ intersect, and even though the energies of the two solutions are the same at this point, the solutions themselves are *distant* in u -space (notice that the stress drops at this point). Hence in order to make a transition from $n = 0$ to $n = 2$, the system has to overcome an *energy barrier* to nucleate a *finite-phase interval* in the *interior* of the bar:

$$(+)\longrightarrow(+, -, +).$$

An energy barrier here means that in order to get from one local minimum of the energy to another with the same boundary conditions the system has to climb up a certain “energy mountain” in u -space.

However, beyond some critical t depending on α and β , the branch unfolds at the point C and the envelope *smoothens up*. Now the transition from $n = 0$ to $n = 2$ occurs *smoothly*:

$$(+)\longrightarrow(+, 0, +)\longrightarrow(+, 0, -, 0, +).$$

First we observe the appearance of a *pretransitional nucleus* in the 0 phase. Then an interval in the $-$ phase (high-strain nucleus) grows gradually inside the

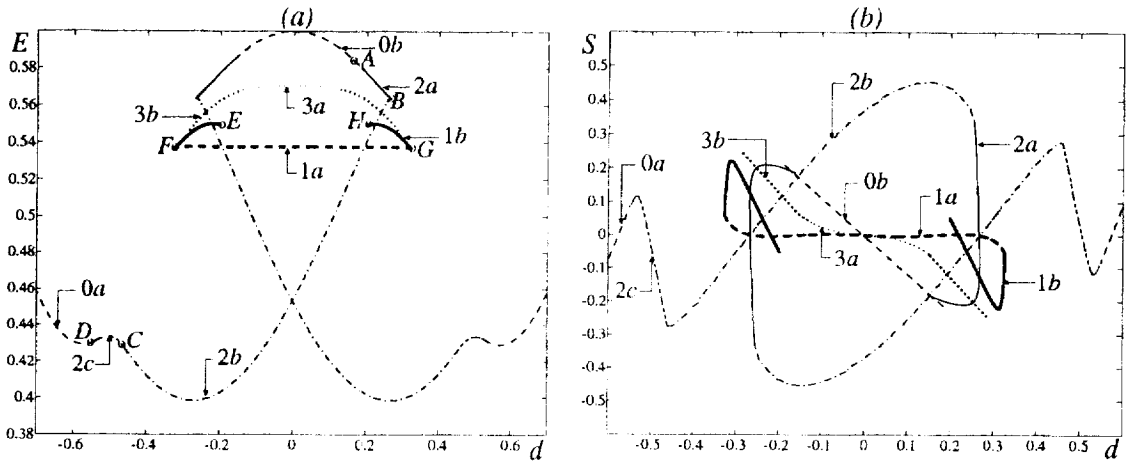


Fig. 11. (a) Energy $E(d)$ and (b) effective stress $S(d)$ diagrams for the three-parabola model: $\alpha = 0.01$, $\beta = 10$, $t = 0.4$; $0a$: (+) (stable), $0b$: (0) (unstable), $1a$: $(-, 0, +)$ (stable), $1b$: $(0, +)$ (unstable), $2a$: $(0, -, 0)$, G-symmetric (unstable), $2b$: $(+, 0, -, 0, +)$, G-symmetric (stable), $2c$: $(+, 0, +)$, G-symmetric (stable), $3a$: $(-, 0, +)$, $n = 3$ (unstable), $3b$: $(0, +)$, $n = 3$ (unstable).

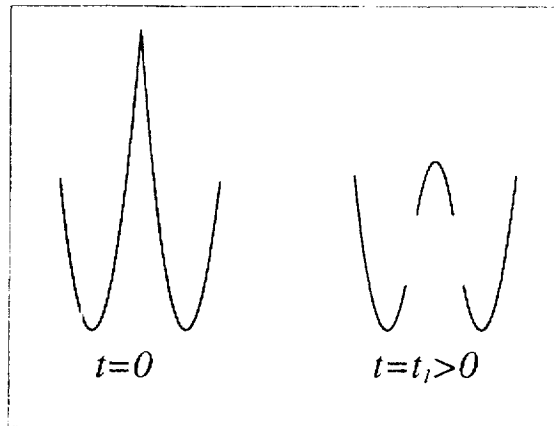


Fig. 12. Sketch of 0-branches.

pretransitional nucleus. Even though there is no energy barrier here in the sense described above, and the system can smoothly get from (+) to $(+, 0, -, 0, +)$ along the path of local minima $(+, 0, +)$ (the segment CD in Fig. 11), the stress still drops before nucleation. This agrees with experimental observations [27].

Another example of a transition from sharp to smooth change of phase due to interactions with the elastic environment is discussed in [5].

5.3.2. Non-G-symmetric branches

Figs. 13 and 14 show the non-G-symmetric $n = 2$ branch $(0, -, 0, +)$ bifurcating from the $n = 2$ symmetric $(0, -, 0)$ branch at the point B (see sketch in Fig. 16(b)) by nucleation of the $+$ phase at one end of the bar (symmetry breaking bifurcation). There is also a $(0, +, 0, -)$ branch bifurcating from $(0, +, 0)$. These correspond to the non-G-symmetric $n = 2$ sub-branches observed in [30] (see Fig. 8). In all three models these branches are unstable.

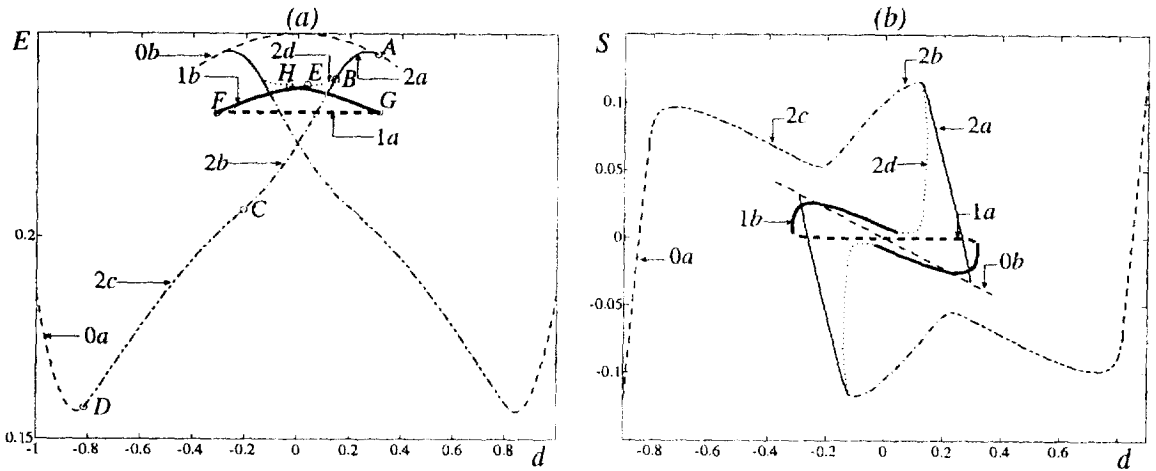


Fig. 13. (a) Energy $E(d)$ and (b) effective stress $S(d)$ diagrams for the three-parabola model: $\alpha = 0.005$, $\beta = 2.3$, $t = 0.75$; $0a$: (+) (stable), $0b$: (0) (unstable), $1a$: (-, 0, +) (stable), $1b$: (0, +) (unstable), $2a$: (0, -, 0), G-symmetric (unstable), $2b$: (+, 0, -, 0, +), G-symmetric (stable), $2c$: (+, 0, +), G-symmetric (stable), $2d$: (0, -, 0, +) (unstable).

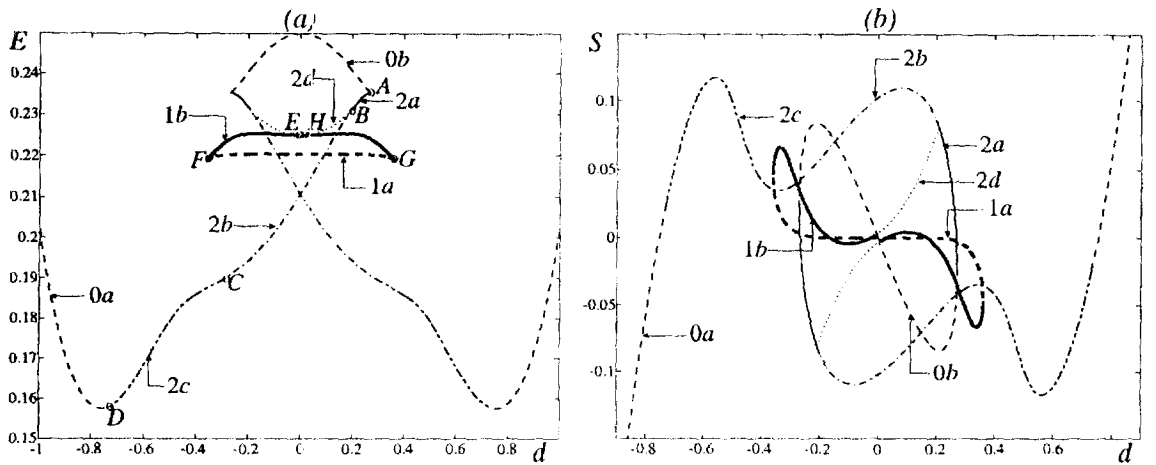


Fig. 14. (a) Energy $E(d)$ and (b) effective stress $S(d)$ diagrams for the fully nonlinear model: $\alpha = 0.005$, $\beta = 2.5$; $0a$: (+) (stable), $0b$: (0) (unstable), $1a$: (-, 0, +) (stable), $1b$: (0, +) (unstable), $2a$: (0, -, 0), G-symmetric (unstable), $2b$: (+, 0, -, 0, +), G-symmetric (stable), $2c$: (+, 0, +), G-symmetric (stable), $2d$: (0, -, 0, +) (unstable).

In Figs. 9–11 we confine our attention to just a few solution branches. In particular, non-G-symmetric $n = 2$ branches are not shown. In these cases there are many equilibria connecting the branches that are shown to the spinodal region part of $n = 0$ as well as to each other in complicated way. Calculating them requires substantial computational effort. We do show all the connections in some cases where n_{\max} is low (Figs. 13, 14 and 17). However, for the cases in

Figs. 9–11, this exhaustive numerical study was not conducted.

5.4. The 1-branches of phase equilibria

In models with a spinodal region the analogs of the $n = 1$ branch in the two-parabola model (see Fig. 8) are of (0, +) and (-, 0, +) type (see Figs. 9–11 and

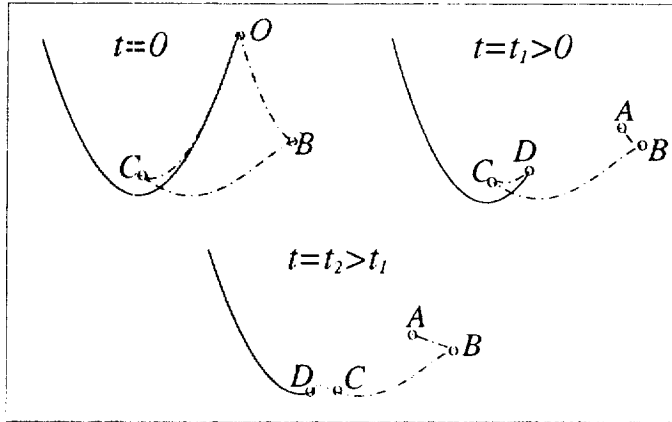


Fig. 15. Sketch of G-symmetric 2-branches: dash-dotted: $n = 2$, solid line: $n = 0$.

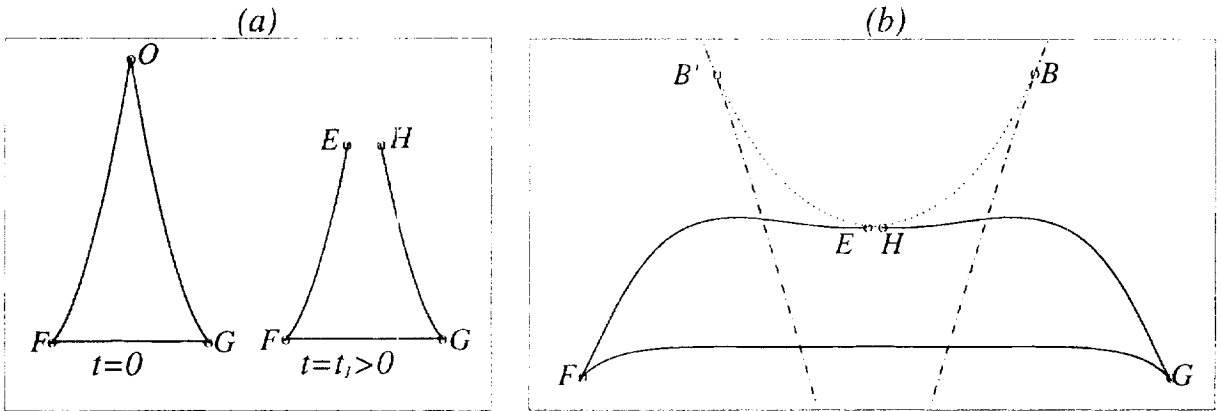


Fig. 16. (a) Sketch of 1-branches. (b) Sketch of non-G-symmetric 2-branches and 1-branches and their connection to the main branch: solid line: $n = 1$, dotted line: $n = 2$, non-G-symmetric, dash-dotted line: $n = 2$, G-symmetric.

Figs. 13 and 14). In the two-parabola model ($t = 0$), the 1-branch has the form of the triangle OFG in Fig. 16. As we increase t , the triangle opens at O ; the sides HG and FE have two different end points E and H rather than O . The curves HG and FE are increasingly occupied by $(0, +)$ -type solutions while the rest of the curve is $(-, 0, +)$ (and corresponding G-related solutions).

Figs. 13 and 14 show how the $n = 1$ branch is connected to the $n = 2$ branch. The following sequence of phase transitions is observed:

$(0, -, 0)$ (symmetric $n = 2$) \rightarrow $(0, -, 0, +)$ (non-symmetric $n = 2$) \rightarrow $(0, +)$ \rightarrow $(-, 0, +)$ \rightarrow $(-, 0)$ \rightarrow $(-, 0, +, 0)$ \rightarrow $(0, +, 0)$. Each branch

is ran over twice by two G-related solutions in all three cases.

Although the energy and stress diagrams for the three-parabola (Fig. 13) and the fully nonlinear model (Fig. 14) differ quantitatively, the shapes of the branches and nucleation patterns are qualitatively similar.

5.5. Solutions with higher number of boundaries

There are cases when solutions with higher n are stable, in addition to the ones discussed above. Thus in Fig. 17 the main branch contains (0) solutions with $n = 2$ and 4 (i.e. strain is in the spinodal region but

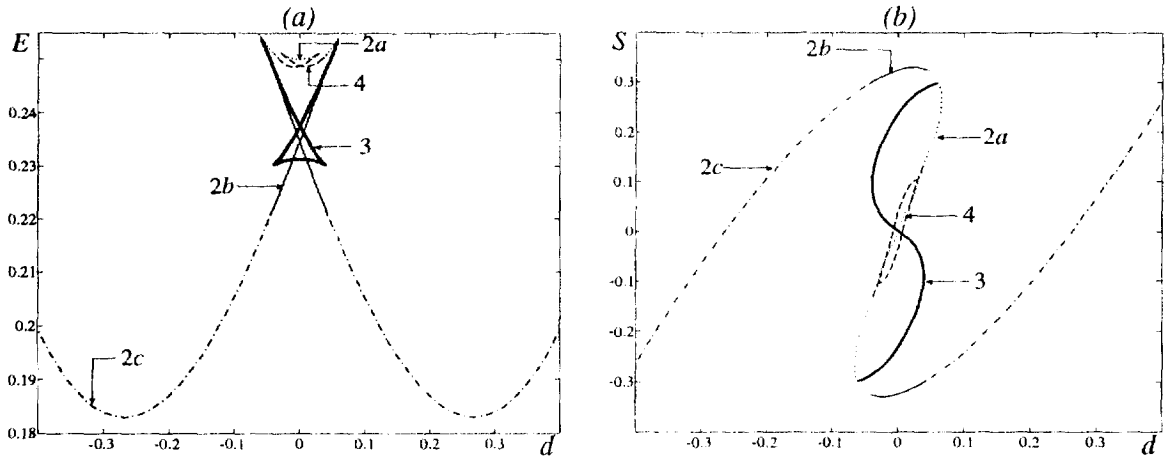


Fig. 17. (a) Energy $E(d)$ and (b) effective stress $S(d)$ diagrams for the fully nonlinear model: $\alpha = 0.0025$, $\beta = 10$; 2a: (0), $n = 2$ (solutions with d between the bifurcation points are unstable, the rest are stable), 4: (0), $n = 4$ (unstable) 2b: (0, -, 0), G-symmetric (stable), 2c: (+, 0, -, 0, +), G-symmetric (stable), 3: (0) \rightarrow (-, 0) \rightarrow (-, 0, +, 0) \rightarrow (-, 0, +, 0, -, 0), $n = 3$ (lowest energy part is stable, upper parts unstable).

intersects zero two and four times respectively). These cannot be observed in the three-parabola model, where the (0) solution is unique for each d . Such underdeveloped solutions are a distinct feature of fully nonlinear energy models. Notice that the (0) solution with $n = 2$ (dotted curve in Fig. 17) is stable right after the bifurcation point. This might correspond to experimentally observed oscillations in strain before phase boundaries appear (“premartensite tweed” [15]). The bifurcating branch contains stable $n = 3$ (-, 0, +, 0, -, 0) solutions.

6. Hysteresis

Although dynamical models would be more appropriate for the study of hysteresis (for instance, one may add a dissipative term u_{xxt} to the stress and include inertia), some observation can be made within our static approach.

For example, consider the stress and energy diagrams in Figs. 14(a) and (b). Following the branches with lowest energy (starting with negative displacement, say, $d = -1$, and then reducing $|d|$), we see that the bar at first has no phase boundaries (+), then (+, 0, +) symmetric solutions evolve, followed by the

truly two-interface (+, 0, -, 0, +) symmetric state. As we approach $d = 0$, there are two possibilities:

- (1) The system follows the lower energy envelope; this will require a drop in stress at $d = 0$ and overcoming a certain energy barrier in order to get from one energy minimizing state (+, 0, -, 0, +) to another (-, 0, +, 0, -).
- (2) The system continues following the (+, 0, -, 0, +) branch for some time, then jumps to another local minimum, e.g. (+, 0, -). If the second possibility occurs, there are different hysteresis paths the system might follow.

A possible approach involves the estimation of barriers. For example, consider the points 1, 2 and 3 on the energy diagram in Fig. 18(a). These represent different equilibria for the same boundary conditions (same d); 1 and 2 are stable and 3 is unstable. One can view 3 as a saddle point or a “mountain pass” between the two minima 1 and 2 (see the schematic at the bottom right corner of Fig. 18(a)). In order to get from state 1 to 2 that has less energy, the system has to overcome a barrier B equal to the difference in the energies of states 1 and 3. We assume that the system jumps from one branch to another when the barrier B is less than or equal to a critical value B_{crit} . When $B_{\text{crit}} = 0.004$, we obtain the hysteresis path

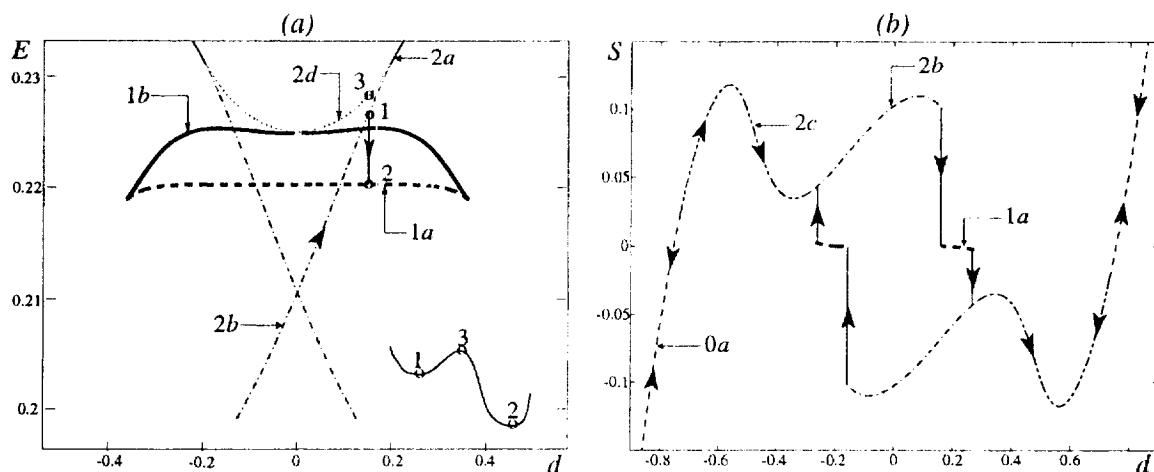


Fig. 18. (a) Estimation of the barrier via unstable solutions. Points 1 and 2 on the energy diagram represent stable solutions (local minima of the total energy), while 3 is an unstable equilibrium. (b) The corresponding hysteresis loop on the stress diagram with the barrier $B_{\text{crit}} = 0.004$. $0a$: (+), $0b$: (0), $1a$: (-, 0, +), $1b$: (0, +), $2a$: (0, -, 0), $2b$: (+, 0, -, 0, +), $2c$: (+, 0, +), $2d$: (0, -, 0, +).

shown in Fig. 18(b). Observe that the system jumps from (+, 0, -, 0, +) to (+, 0, -) first, and then to (-, 0, +, 0, -). Although the (-, 0, +, 0, -) branch has lower energy than (+, 0, -), the system does not switch to it right away because the barrier is too high ($B = 0.015$). The hysteresis loop is wider for smaller values of B_{crit} .

7. Conclusions

Our study shows that the presence of a spinodal region in phase transition models that incorporate non-local interactions has a strong effect on nucleation mechanisms and resulting microstructures.

We find that in models with sufficiently wide spinodal region an *infinitesimal* phase nucleation in the *interior* of the bar is possible. The system makes the transition from $n = 0$ to $n = 2$ through the formation of a “premartensite” structure in the interior. This happens by the appearance and growth of a *pretransitional* nucleus of the 0 phase inside the low-strain phase, followed by the appearance of a high-strain nucleus within the former. This process has some characteristics of a second-order phase transition. The effect cannot be captured by the two-parabola model (or a model with a narrow spinodal region) where only

sudden *finite* phase nucleation can occur. Accordingly, in models with wide spinodal region, the *lowest energy envelope smoothens*. Another kind of nucleation – with a *finite* nucleus at one of the *boundaries* of the bar – can still take place in models with a spinodal region. These transitions are *nonsmooth* as predicted in [30]; the system has to overcome an energy barrier in jumping from one state to another. As a result, the overall lowest energy envelope is only piecewise smooth even in models with spinodal region. This leads to discontinuities on the corresponding stress diagram [10,30].

The size and shape of the spinodal region determine the (finite) maximum number of phase boundaries in bifurcating equilibria. Recall that this number is infinite in the two-parabola model. Due to the degeneracy of the latter, all branches of equilibria bifurcate from the $u = 0$ solution point at $d = 0$. In smoother models the structure of connections between equilibrium branches unfolds. It is remarkable, however, that stability results are similar in all three models.

The results of numerical computations for the fully nonlinear model and semianalytical results for the three-parabola model are in qualitative agreement. This implies that the three-parabola model captures the main effects of the spinodal region.

Our work suggests that, apart from dynamics, there are purely energetic reasons for the hysteresis

phenomenon. We remark that more sophisticated models of the elastic foundation (for example, when Ericksen's bar is coupled with a linearly elastic bar by a "springy glue") yield hysteresis loops that are in better qualitative agreement with experimental observations. These models are currently under investigation.

Acknowledgments

This research was supported by the National Science Foundation through grants DMS-9625830 (TH), MSS-9312858 (PR) and DMS-9501433 (LT). We would also like to thank A. Polyakov whose computer code was adapted for the three-parabola calculations.

References

- [1] R. Abeyaratne, C. Chu, R.D. James, Kinetics and hysteresis in martensitic single crystals, in: *Mechanics of Phase Transformations and Shape Memory Alloys*, ASME, New York, 1994.
- [2] J.M. Ball, C. Chu, R.D. James, Hysteresis during stress-induced variant rearrangement, *J. Physique* 5 (8) (1995).
- [3] J.M. Ball, P.J. Holmes, R.D. James, R.L. Pego, P.J. Swart, On the dynamics of fine structure, *J. Nonlinear Sci.* 1 (1991) 17–70.
- [4] D. Brandon, T. Lin, R. Rogers, Phase transitions and hysteresis in nonlocal and order parameter models, *Meccanica* 30 (1995) 541–565.
- [5] B. Budiansky, L. Truskinovsky, On the mechanics of stress-induced phase transformation in zirconia, *J. Mech. Phys. Solid* 41 (9) (1993) 1445–1459.
- [6] J. Carr, M.E. Gurtin, M. Slemrod, Structured phase transitions on a finite interval, *Arch. Rat. Mech. Anal.* 86 (1984) 317–351.
- [7] C. Chu, Hysteresis and microstructures: A study of biaxial loading on compound twins of copper–aluminum–nickel single crystals, Ph.D. Thesis, University of Minnesota, 1993.
- [8] E.J. Doedel, J.P. Kerneves, AUTO: Software for continuation and bifurcation problems in ordinary differential equations, 1986.
- [9] J.L. Ericksen, Equilibrium of bars, *J. Elasticity* 5 (1975) 191–202.
- [10] B. Fedelich, G. Zanzotto, Hysteresis in discrete systems of possibly interacting elements with a two well energy, *J. Nonlinear Sci.* 2 (1992) 319–342.
- [11] S. Fu, I. Müller, H. Xu, The interior of the pseudoelastic hysteresis, in: C.Y. Liu, H. Kunsmann, K. Otsuka, M. Wuttig (Eds.), *Mat. Res. Soc. Symp. Proc.*, vol. 246, 1992, pp. 39–42.
- [12] T.J. Healey, Global bifurcation and continuation in the presence of symmetry with an application to solid mechanics, *SIAM J. Math. Anal.* 19 (4) (1988) 824–840.
- [13] R.D. James, Deformation of shape-memory materials, in: C.Y. Liu, H. Kunsmann, K. Otsuka, M. Wuttig (Eds.), *Mat. Res. Soc. Symp. Proc.* vol. 246, 1992, pp. 81–90.
- [14] I. Kaganova, A. Roitburd, Equilibrium shape of an inclusion in a solid, *Sov. Phys. Dokl.* 32 (1987) 925–927.
- [15] S. Kartha, J.A. Krumhansl, J.P. Sethna, L.K. Wickham, Disorder driven pretransitional tweed pattern in martensitic transformations, *Phys. Rev. B* 52 (2) (1995) 803.
- [16] D. Kinderlehrer, L. Ma, The hysteretic event in the computation of magnetization and magnetostriction, in: H. Brezis, J.-L. Lions (eds.) *Proc. Nonlinear Diff. Eqns. and Their Appl.*, College de France Sem., 1994.
- [17] B. Li, Unpublished notes; private communication, 1995.
- [18] I.M. Lifshitz, Macroscopic description of twinning phenomena in crystals, *Sov. Phys. JETP* 18 (1948) 1134–1152.
- [19] A.E. Lifshitz, G.L. Rybnikov, Dissipative structures and couette flow in a non-newtonian fluid, *Sov. Phys. Dokl.* 30 (4) (1985) 275–278.
- [20] S. Müller, Minimizing sequences for nonconvex functionals, phase transitions and singular perturbations, *Lecture Notes in Physics*, vol. 359, Springer, Berlin, 1990, pp. 31–44.
- [21] S. Müller, Singular perturbation as a selection criterion for periodic minimizing sequences, *Calculus of Variations* 1 (1993) 169–204.
- [22] I. Müller, P. Villaggio, A model for an elastic–plastic body, *Arch. Rat. Mech. Anal.* 65 (1977) 25–46.
- [23] A. Novick-Cohen, L.A. Segel, Nonlinear aspects of the Cahn–Hilliard equation, *Physica D* 10 (1984) 277–298.
- [24] R. Rogers, L. Truskinovsky, Discretization and hysteresis, *Physica B* 233 (1997) 370–375.
- [25] P. Rosakis, Compact zones of shear transformation in an anisotropic solid, *J. Mech. Phys. Solids* 40 (1992) 1163–1195.
- [26] D. Schryvers, Y. Ma, L. Toth, L. Tanner, Nucleation and growth of bainitic Ni₅Al₃ in B2 austenite, in: *PTM Solid–Solid Phase Transitions*, 1994.
- [27] J.A. Shaw, S. Kyriakides, On the thermomechanical behavior of NiTi, Technical Report 94/12, EMRL, Department of Aerospace Engineering and Engineering Mechanics, The University of Texas at Austin, 1994.
- [28] N. Triantafyllidis, S. Bardenhagen, On higher order gradient continuum theories in 1-D nonlinear elasticity. Derivation from and comparison to the corresponding discrete models, *J. Elasticity* 33 (3) (1993) 259–293.
- [29] L. Truskinovsky, G. Zanzotto, Finite-scale microstructures and metastability in one-dimensional elasticity, *Meccanica* 30 (1995) 577–589.
- [30] L. Truskinovsky, G. Zanzotto, Ericksen's bar revisited: Energy wiggles, *J. Mech. Phys. Solids* 44 (8) (1996) 1371–1408.
- [31] L.C. Young, *Lectures on the Calculus of Variations and Optimal Control Theory*, Chelsea, New York, 1980.
- [32] E. Zeidler, *Nonlinear Functional Analysis and its Applications*, vol. III, Springer, Berlin, 1984.